Eur. Phys. J. D **19**, 395–402 (2002)
DOI: 10.1140/epjd/e20020085

THE EUROPEAN PHYSICAL JOURNAL D
EDP Sciences

Third-order nonlinear optical response of Au:SiO_2 thin films: Influence of gold nanoparticle concentration and morphologic parameters

N. Pinçon, B. Palpant[a], D. Prot, E. Charron, and S. Debrus

Laboratoire d'Optique des Solides, CNRS - Université Pierre et Marie Curie, Case 80, 4 place Jussieu, 75252 Paris Cedex 05, France

Received 12 December 2001

Abstract. We report a study on the third-order nonlinear optical properties of nanocomposite thin films composed of gold particles embedded in a silica host matrix. Samples of various metal volume fractions, ranging from 8 to 35%, are synthesized by the sputtering technique. Some of them are annealed. Nonlinear optical measurements, which are performed by using the z-scan technique, reveal both a very large nonlinear absorption and a weak nonlinear refraction close to the surface plasmon resonance frequency of the particles. We especially study the effect of the metal concentration and the influence of thermal treatment on the real and imaginary components of the third-order nonlinear susceptibility. Our results reveal that, as the metal concentration reaches a few percent, the mutual electromagnetic interactions between particles greatly enlarge the nonlinear optical response of the material and can not be neglected in the theoretical analysis. Moreover, the thermal treatment leads, for a given concentration, to a significant increase of the nonlinear response, which is ascribed to a modification of the material morphology. We finally point out that the material nonlinear properties are very sensitive to the incident wavelength through the local field enhancement phenomenon.

PACS. 78.67.Bf Nanocrystals and nanoparticles – 42.65.An Optical susceptibility, hyperpolarizability – 61.46.+w Nanoscale materials: clusters, nanoparticles, nanotubes, and nanocrystals

1 Introduction

The linear optical properties of nanocermets (standing for "ceramic-metal") consisting of noble metal nanoparticles embedded in a dielectric host have been extensively studied for many years. The main feature in the linear optical response of these materials is the excitation of the surface plasmon resonance (SPR), which induces an absorption band whose amplitude, spectral location and width depend on the metal particle size, shape and concentration in the medium [1]. The SPR is responsible for the enhancement of the local electromagnetic field in the particles, which induces an amplification of their nonlinear properties as compared to those of bulk metal [2,3]. This explains the large effective third-order nonlinear susceptibility, $\chi^{(3)}$, of nanocermets. Like their linear optical response, the nonlinear response of such media depends drastically on both the intrinsic particle characteristics and the nature of the host medium through the local field enhancement process linked with the SPR [4–25].

Thanks to this high nonlinear optical response, nanocermets are thought to be good potential candidates to be used in new photonics devices, such as all-optic switching or routing units, provided the sign and the relative weight of the real and imaginary parts of $\chi^{(3)}$ meet the technological needs. Nevertheless, many experimental studies devoted to the measurement of the nonlinear properties of nanocomposite media have been realized by using the DFWM (degenerate four-wave mixing) technique, which can only provide the modulus of the third-order susceptibility [5,7,11,13,14,17,18,21].

The first studies devoted to the measurement of $\chi^{(3)}$ were carried out on very weakly concentrated colloidal solutions of gold nanoparticles [2,3]. Nowadays, physical and chemical synthesis techniques enable the elaboration of materials containing higher metal amounts. It is thus of interest to investigate the effect of metal concentration on the nonlinear optical properties [13,17]; indeed, the mutual interaction between particles (increasing as the concentration increases) can result in a strong additional enhancement of the local field, and then in an amplification of the nonlinear response. In a previous article we presented a study of the third-order nonlinear susceptibility of a nanocermet thin film composed of gold particles embedded in a SiO_2 matrix [24]. The present paper is focused on the link between selected morphologic parameters and the nonlinear properties. The influence of metal concentration on the value of the real and imaginary components

[a] e-mail: palpant@ccr.jussieu.fr

of $\chi^{(3)}$ has been especially analyzed. Moreover, the effect of the material heat treatment on the optical properties has been investigated through the changes induced in the cermet morphology.

Thin films consisting of gold particles embedded in a SiO_2 matrix have been prepared by radio-frequency sputtering with different metal volume fractions. Information about the thin film morphology are provided by different characterization techniques. Spectrophotometric and ellipsometric measurements enable to determine the nanocermet effective linear complex index. The nonlinear optical response is then measured close to and off resonance by the z-scan technique [26] which offers the great advantages, over the DFWM one providing $|\chi^{(3)}|$ only, to get simultaneously the real and imaginary parts of $\chi^{(3)}$ together with their sign [8–10,15,16,20,22].

2 Preparation and morphologic characterizations of Au:SiO_2 thin films

Au:SiO_2 cermets have been synthesized by radio-frequency sputtering in a vacuum chamber (2×10^{-5} torr) as thin films deposited on a substrate [27,28]. The target-to-substrate distance is fixed at 6 cm. The target consists of a pure SiO_2 disc (99.998% purity, 13 cm diameter) with a gold sector plated on it. The rotation of the substrate holder enables an alternating deposition of granular gold and SiO_2. The synthesis process parameters (rare gas partial pressure, sputtering power, substrate rotation speed) are chosen as to obtain the desired film thickness and metal concentration. Several samples have been prepared with various gold volume fractions under the percolation threshold. Part of them have subsequently been annealed at 800 °C during one minute in a rapid annealing furnace. Different substrate types have been used, depending on the characterizations and measurements to be carried out: silica plates, monocrystalline silicon wafers, carbon-coated copper grids for TEM (transmission electron microscopy).

The samples have then been characterized by different techniques. The cross sectional TEM micrograph shown in Figure 1 has been obtained by the ion beam milling method. This reveals isolated gold clusters randomly dispersed in the host matrix. It shows that almost all particles are spherical, result which is confirmed by GISAXS (grazing incidence small-angle X-ray scattering) [29]. As can be observed, the film synthesis technique ensures a homogeneous distribution of the gold clusters in depth, for both metal concentration and particle size. The apparent concentration increase from the edge to the substrate sides of the film actually stems from the transverse gradient induced by the ionic milling.

The accurate value of the film thickness and the metal volume fraction, already roughly estimated before the synthesis process, have been deduced from α-step profilometry and RBS (Rutherford back-scattering spectroscopy) measurements, respectively. The metal concentration varies between 8 and 35% from sample A to sample D; the film thickness, chosen as to get roughly the same

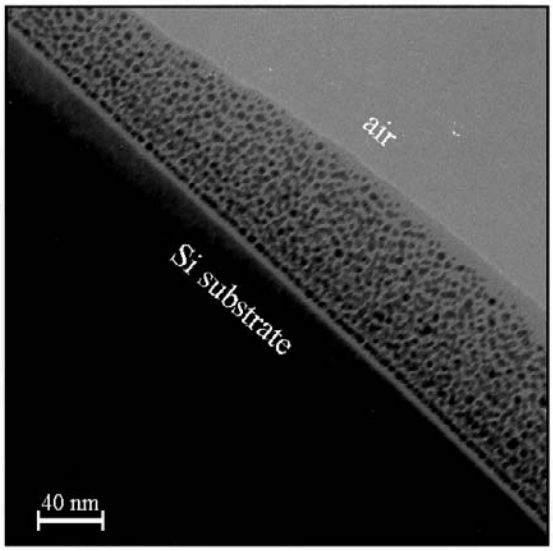

Fig. 1. Cross-sectional TEM micrograph of an Au:SiO_2 thin film (thickness: 70 nm) with metal volume fraction $p = 23\%$ (sample C).

total optical transmission T from one sample to another ($T \sim 0.3$), ranges within 60 and 180 nm. The comparison of the real film thickness and the one deduced from the fitting of the RBS measurements allows to evaluate the porosity of the silica matrix, which is worth $17 \pm 9\%$.

The mean particle size has been determined by GISAXS for the as-deposited and the annealed samples. These measurements reveal a mean particle diameter ranging from 2.6 to 4.8 nm depending on the sample, as well as a 0.2 nm small increase after annealing (only sample D was not annealed), the particles remaining spherical. The film metal concentration and mean particle size are reported in Table 1 for all samples. GISAXS measurements also exhibit a typical feature signing the existence of spatial correlations between particles in each annealed sample [29,30]. It is linked with a more homogeneous spatial distribution of particles in the host matrix after heat treatment. The mean distance between particles, which is deduced from the spatial correlation signal, is also reported in Table 1. As expected, this distance decreases with increasing concentration. The thermal annealing also results in the improvement of the crystalline quality of metal particles [31]. This effect was in particular observed using X-ray diffraction by Tanahashi *et al.* [11] who measured more intense gold diffraction peaks after heat treatment of films containing gold particles. Duval *et al.* [32] also showed by high-resolution TEM a large decrease of the lattice defects in silver clusters after annealing at 800 °C or 1 000 °C.

3 Linear optical propreties of the samples

The linear optical response of the samples is characterized by their effective linear index $\tilde{n}(\lambda)$ or their effective

Table 1. Morphologic parameters (metal concentration, mean particle size, mean distance between neighboring particles) of both as-prepared and annealed samples A to D.

Sample		Metal volume fraction (%)	Particles mean diameter (nm)	Mean distance between particles (nm) [a]
A	as-deposited	8	2.6	–
	annealed		2.8	9.0
B	as-deposited	16	2.8	–
	annealed		3.0	8.0
C	as-deposited	23	3.0	–
	annealed		3.2	7.5
D [b]	as-deposited	35	4.8	–

[a] The value is given only when a clear correlation signal can be found in the GISAXS result (see text).
[b] Sample D has not been elaborated by multilayer deposition but by co sputtering with a SiO_2 target on which gold pellets were plated following an hexagonal array. Other deposition parameters have been kept the same as for multilayer technique. This sample has not been annealed.

linear dielectric function $\varepsilon(\lambda) = \tilde{n}^2(\lambda)$. $\tilde{n}(\lambda)$ can be written as $\tilde{n}(\lambda) = n_0(\lambda) + \mathrm{i}\alpha_0(\lambda)/2k$, where λ is the incident light wavelength, $n_0(\lambda)$ is the refraction index, $\alpha_0(\lambda)$ the absorption coefficient and $k = 2\pi/\lambda$ the modulus of the wave vector. Beyond the proper interest in understanding these linear properties, the knowledge of $\tilde{n}(\lambda)$ is necessary for the calculation of $\chi^{(3)}$ from the z-scan experiment results. This has led us to carry out spectrophotometric and ellipsometric measurements. Transmission and reflection spectra have been recorded in the spectral range 300–1 000 nm with a Varian (Cary 5) spectrophotometer for the films deposited on silica substrates. The linear absorption coefficient $\alpha_0(\lambda)$ and the corresponding refractive index $n_0(\lambda)$ have then been extracted by means of a commercial fitting software (Film Wizard$^{\mathrm{TM}}$, Sci). Ellipsometric measurements have been performed in the spectral range 300–800 nm with a Sopra ellipsometer for the samples deposited on silicon substrates. Both types of measurements give similar results for $\tilde{n}(\lambda)$. The spectra are shown in Figures 2a and 2b. The absorption coefficient profile reveals an absorption band in the visible domain – originating from the SPR phenomenon – the maximum of which ranges within $\lambda = 495$ and 555 nm. Figure 2b exhibits also the increase of the SPR band relative amplitude with increasing metal volume fraction. The precise location of the band maximum as well as the bandwidth and amplitude – and more generally the whole profile of both $n_0(\lambda)$ and $\alpha_0(\lambda)$ – for the different samples are ruled by the subtle concomitance of different effects, namely:

(i) quantum size effects (involving not only conduction electrons but also core electrons from the d band in the case of noble metals nanoparticles) [1,33];
(ii) porosity of the matrix (which can modify the local environment of the particles and thus their optical response) [34];
(iii) and influence of metal concentration (which actually reflects the influence of mutual interactions between particles and can be treated in a first approach by mean field theories) [1,35–37].

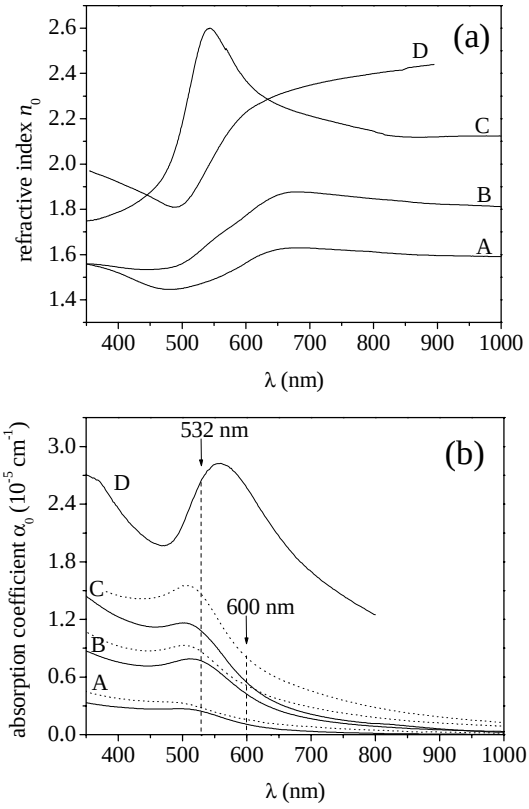

Fig. 2. Spectral variation of the optical linear index for the four Au:SiO_2 thin films. Labels correspond to those in Table 1. (a) Refractive index $n_0(\lambda)$ and (b) absorption coefficient $\alpha_0(\lambda)$ of the as-deposited (solid line) and annealed (dotted line) films.

Moreover, one can notice in Figure 2 that the profiles of the linear refractive index and absorption coefficient of sample D look rather different than those of the other samples; this is due to its high metal concentration, close to the percolation threshold, for which the optical properties are strongly modified as compared to the case of lower p values [37,38].

Table 2. Nonlinear absorption measurement results close to (532 nm) and off (600 nm) SPR. The imaginary part of $\chi^{(3)}$ is reported for the as-deposited and annealed samples.

	Sample	$\mathrm{Im}\chi^{(3)}$ ($\times 10^{-6}$ esu)	
		$\lambda = 532$ nm	$\lambda = 600$ nm[a]
A	as-deposited	-0.049 ± 0.009	0
	annealed	-0.69 ± 0.06	0
B	as-deposited	-0.76 ± 0.25	0
	annealed	-1.5 ± 0.5	0
C	as-deposited	-3.0 ± 0.8	0
	annealed	-6.0 ± 0.6	0
D	as-deposited	-6.4 ± 1.2	not measured

[a] Zero value means that the value is weaker than our apparatus sensitivity.

The absorption curves of the annealed films (samples A to C) are also shown as dotted lines in Figure 2b. One can observe an overall increase of the absorption after sample annealing. This increase can be explained by considering the amount of metal taking part in the optical response as gold nanoparticles. Indeed, isolated gold atoms dispersed in the dielectric host, which primarily do not contribute to the optical response of the as-deposited films in the SPR spectral domain, can diffuse and coalesce into clusters under thermal treatment, thus increasing the amount of "optically active" metal. Furthermore, the SPR absorption band itself experiences a slight relative amplitude increase as well as a slight narrowing after annealing, this feature being especially pronounced for sample C. These enhancement and narrowing can be explained by the modification, induced by the heat treatment, of the effective damping parameter Γ for the free electrons in the metal spheres. Indeed, this parameter plays a crucial role in the expression of the conduction electrons contribution to the metal dielectric function (Drude model), which is given by:

$$\varepsilon(\omega) = 1 - \frac{\omega_\mathrm{p}^2}{\omega^2 + \mathrm{i}\Gamma\omega}, \tag{1}$$

where ω_p is the volume plasma frequency. Classical and quantum models devoted to the study of the SPR bandwidth in small particles have led to express Γ as [1]:

$$\Gamma(r) = \Gamma_\infty + \frac{A\nu_\mathrm{F}}{r} \tag{2}$$

where Γ_∞ is the bulk damping constant (electron interactions with impurities, lattice defects, other electrons, phonons), ν_F is the Fermi velocity and A is a model-dependent parameter. This bandwidth size dependence is often viewed, in a classical picture, as the effect of the reduction of the electron mean free path when confined in particles whose size is smaller than the bulk mean free path, typically in the range of few tens of nanometers [1]. The modification of $\Gamma(r)$ through the modification of both Γ_∞ and r can explain the changes in the absorption band observed after heat treatment: on the one hand the decrease of defects concentration, as discussed in Section 2, results in the weakening of Γ_∞ [39]; on the other hand the slight size increase induced by annealing (see Tab. 1) results in a decrease of the damping constant following equation (2). Therefore, a better crystalline quality and an increase of the particle size give rise to the plasmon band enhancement and narrowing.

4 Experimental study of the effective third-order nonlinear susceptibility

The effective third-order nonlinear susceptibility of the Au:SiO_2 cermets has been measured by the z-scan technique [24,26] which allows to measure simultaneously the real and imaginary parts of $\chi^{(3)}$ together with their respective sign. The sample is moved along the axis z of a focused Gaussian-profile laser beam, the power of which is kept constant during the whole scan. The incident light intensity I is maximum at the beam waist, and decreases as the sample moves away from it. The variations of the total flux transmitted by the sample, measured by a photodiode as a function of the sample distance z from the waist, can then be related to the nonlinear absorption coefficient β, which is defined by writing the total light absorption by the sample as:

$$\alpha(I) = \alpha_0 + \beta I. \tag{3}$$

β is proportional to the imaginary part of $\chi^{(3)}$ as:

$$\beta = \frac{3k\ \mathrm{Im}\chi^{(3)}}{2\varepsilon_0 c n_0^2}\cdot \tag{4}$$

A small aperture placed in far-field before the detector enables to measure beam distortions induced by the sample nonlinear refractive index. One can thus deduce the nonlinear refraction coefficient γ which is defined by writing the sample total refractive index as:

$$n(I) = n_0 + \gamma I \tag{5}$$

γ is proportional to the real part of $\chi^{(3)}$ as:

$$\gamma = \frac{3\ \mathrm{Re}\chi^{(3)}}{4\varepsilon_0 c n_0^2}\cdot \tag{6}$$

Measurements have been performed using a frequency-doubled Q-switched Nd:YAG laser providing 7 ns-duration pulses at 532 nm with a 10 Hz repetition rate. The laser has also been used as a pump of a dye laser in order to measure $\chi^{(3)}$ at different excitation wavelengths.

The nonlinear absorption and refraction coefficients have been measured at 532 nm, that is close to the SPR absorption band, and at 600 nm, in the red wing of the absorption band (see arrows in Fig. 2b). The linear index determined previously (see Sect. 3) is used for the calculation of $\chi^{(3)}$ from the z-scan experiment results (*i.e.* β and γ, see Eqs. (4, 6)).

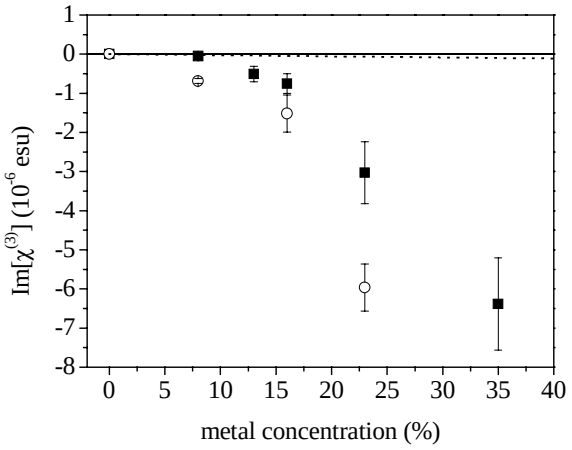

Fig. 3. Variation of $\mathrm{Im}\chi^{(3)}$ as a function of gold concentration, for both the as-deposited (squares) and annealed (circles) samples. The dashed line corresponds to the dilute media theory (Eqs. (7, 8)).

At 532 nm, we have measured for each film a negative nonlinear absorption coefficient revealing an absorption saturation phenomenon in the neighborhood of the SPR peak maximum. Measurements give β values ranging from -0.23×10^{-3} to -22.3×10^{-3} cm/W for the as-deposited samples and from -2.8×10^{-3} to -18.3×10^{-3} cm/W for the annealed samples (except sample D which was not annealed), the metal volume fraction increasing from 8% to 35%. These results lead (Eq. (4)) to values of $\mathrm{Im}\chi^{(3)}$ ranging from $-(0.049\pm0.009)\times10^{-6}$ esu (sample A) to $-(6.4\pm1.2)\times10^{-6}$ esu (sample D) for the as-deposited thin films. After annealing it gives values from $-(0.69\pm0.06)\times10^{-6}$ esu (sample A) to $-(6.0\pm0.6)\times10^{-6}$ esu (sample C). These results are obtained by averaging the β values measured on different points and at different laser powers for each sample.

The variations of $\mathrm{Im}\chi^{(3)}$ measured at 532 nm as a function of the metal volume fraction p are shown in Figure 3. Squares and circles correspond to the as-deposited and annealed samples, respectively. Results reveal a large enhancement of $\mathrm{Im}\chi^{(3)}$ with increasing p: a hundred-fold increase in $\mathrm{Im}\chi^{(3)}$ as the metal concentration rises from 8 to 35%. One can notice that with increasing metal amount, the experimental results diverge from the theoretical prediction (solid line in Fig. 3) suited for weakly concentrated materials. This theoretical curve, determined in the quasi-static approximation through a mean-field approach, is derived from the following expression [4]:

$$\chi^{(3)}(\omega) = p|f(\omega)|^2 f^2(\omega)\chi_{\mathrm{m}}^{(3)}(\omega), \tag{7}$$

where $\chi_{\mathrm{m}}^{(3)}$ is the intrinsic third-order nonlinear susceptibility of gold particles. Its value, measured by Smith *et al.* at 532 nm on a bulk gold film [40], was taken as equal to $\chi_{\mathrm{m}}^{(3)} = (-1+5\mathrm{i})\times10^{-8}$ esu. The intrinsic nonlinear properties of the particles result from three main physical contributions [2,4,10]:

(i) *the interband* one, stemming from – as already mentioned in Section 3 – the electronic transitions from the fulfilled *d* band to the *sp* band;
(ii) *the hot electron* contribution or, in other words, the modification of the optical properties due to the strong raise of the electronic temperature subsequent to the absorption of light (modification of the Fermi-Dirac distribution);
(iii) and *the intraband* contribution, due to the confinement of the conduction electrons in the nanoparticles.

This last term, absent of course in bulk metal, is anyway expected to be low as compared to the two others in the case of small particles [2,4].

The other quantity appearing in the above equation, *f*, called the local field factor, is the ratio between the field in a metal particle and the applied field. Its value in the case of a weak metal concentration is obtained by calculating the electric field in an isolated particle in the quasi-static limit:

$$f(\omega) = \frac{3\varepsilon_{\mathrm{d}}(\omega)}{\varepsilon'_{\mathrm{m}}(\omega) + 2\varepsilon_{\mathrm{d}}(\omega) + \mathrm{i}\varepsilon''_{\mathrm{m}}(\omega)}, \tag{8}$$

where $\varepsilon_{\mathrm{d}}(\omega)$ is the dielectric function of the dielectric host matrix, $\varepsilon'_{\mathrm{m}}(\omega)+\mathrm{i}\varepsilon''_{\mathrm{m}}(\omega)$ the dielectric function of the bulk metal. Equation (7) predicts a linear variation of $\mathrm{Im}\chi^{(3)}$ with metal concentration and a local-field dependence. Our measurements reveal that $\mathrm{Im}\chi^{(3)}$ does not vary linearly with p, stemming from the fact that as soon as p reaches a few percent, mean field theories – which neglect spatial fluctuations of the electric field on the mesoscopic scale – can not be applied any more. It has been also suggested [7] that $\chi^{(3)}$ is proportional to both p and the fourth power of the particle radius, or to both the fourth power of the linear coefficient at SPR maximum, $\alpha_{\max}$ and the inverse cube of p. No such dependence has been clearly evidenced from our measurements. Moreover, as the intrinsic susceptibility of the metal particles, $\chi_{\mathrm{m}}^{(3)}$, has been shown to be weakly size dependent (since dominated by the interband and possibly hot electron contributions, as compared to the intraband one) [4,5,9] and as the mean radius evolution in our experiment is small from one sample to another (see Tab. 1), the strong variation of $\mathrm{Im}\chi^{(3)}$ with metal concentration reported in Figure 3 can be mainly assigned to the enhancement of the local electromagnetic field. These experimental results underline the necessity of performing accurate local field enhancement calculations by taking into account the mutual influence between particles, in order to better predict the magnitude of the third-order nonlinear response of highly concentrated cermets, as it has already been demonstrated by Shalaev *et al.* in the case of two-dimensional granular films [41,42]. Let us notice that, due to these effects, it would have no sense to extract from our measurements the value of the particle third-order susceptibility, $\chi_{\mathrm{m}}^{(3)}$, by using equation (7), whereas such an assessment is justified in the case of weakly-concentrated media (doped glasses, colloidal solutions, ...) [4,5,9,11,16,22,25].

Figure 3 also exhibits a significant increase of $\mathrm{Im}\chi^{(3)}$ after annealing for all samples. This effect can be ascribed, as for the linear optical response, to enhancement of the local electric field in the metal particles at the SPR after heat treatment (see Sect. 3). It is noteworthy that, whereas the local field enhancement factor $f(\omega)$ at the SPR experiences modifications due to changes in the material morphology, the nonlinear optical response amplifies these modifications since the modulus of the third-order effective susceptibility varies – at least for weakly concentrated media – as $\sim |f(\omega)|^4$ (Eq. (7)).

Let us now discuss the z-scan measurements performed with the aperture in the far-field in order to determine the real part of the nonlinear susceptibility, $\mathrm{Re}\chi^{(3)}$. Measurements performed at 532 nm, that is close to the SPR band maximum, show that $\mathrm{Re}\chi^{(3)}$ is too weak to be precisely measurable. Two reasons can throw light on the lack of nonlinear refractive index signal. At first, the large nonlinear absorption prevents from detecting, on the z-scan curve, the beam phase distortion induced by the nonlinear refraction. This limit of the z-scan technique in the case of materials with very large nonlinear absorption has already been discussed in reference [24]. Secondly, $|\mathrm{Re}\chi^{(3)}|$ is expected to be very weak when $|\mathrm{Im}\chi^{(3)}|$ is close to its maximum. As pointed out by Hache *et al.* [4], in the spectral domain around $\lambda = 532$ nm, the third-order susceptibility of bulk gold $\chi^{(3)}_{\mathrm{m}}$ is mainly imaginary ($|\mathrm{Im}\chi^{(3)}_{\mathrm{m}}|$ is five times higher than $|\mathrm{Re}\chi^{(3)}_{\mathrm{m}}|$ as found by Smith *et al.* [40]). However, due to local field corrections, the effective nonlinear susceptibility of nanocermets has to be examined more carefully before concluding on the sign and value of both its real and imaginary components. Indeed, even if the local field factor in the case of highly metal-concentrated media is no more given by the simple equation (8) due to mutual interaction between neighboring particles as stated before, the complex value of the material effective $\chi^{(3)}$ depends on both the real and imaginary parts of $f(\omega)$ which experience strong variations around the SPR frequency. As an illustration, the modulus of the local field factor f, calculated following equation (8), as well as the real and imaginary parts of $\chi^{(3)}$ as given by equation (7) for an Au:SiO_2 nanocermets with $p = 10\%$ are plotted against incident wavelength λ in Figures 4a and 4b. The complex $\chi^{(3)}_{\mathrm{m}}$ value found by Smith *et al.* [40] for bulk gold has been used. Let us recall that, in this calculation, f is evaluated for a single metal sphere surrounded by the host matrix, that is, no local mutual interaction effects between particles or even no effective medium effects are taken into account. Moreover, due to quantum size effects, the SPR band would be shifted and broadened and, consequently, so would be the spectral profile of the features attached to both $\mathrm{Re}\chi^{(3)}$ and $\mathrm{Im}\chi^{(3)}$. This plot should then be considered only as a qualitative basis for discussion. One can nonetheless see that, due to the combination of both $\chi^{(3)}_{\mathrm{m}}$ and f complex values, it is possible to get high negative $\mathrm{Im}\chi^{(3)}$ value together with a much weaker $\mathrm{Re}\chi^{(3)}$ value at some wavelengths close to the SPR. This feature certainly explains that, once removed the high nonlinear absorption effect superimposed on the signal recorded through the small aperture in the z-scan experiment, the remaining signal linked with beam phase distortions induced by nonlinear refraction is too weak to assess the coefficient γ significantly. In our previous paper, we could only give an upper value for the real part of the third-order susceptibility of a Au:SiO_2 cermet with $p = 20\%$, $\mathrm{Re}\chi^{(3)} \leq 1.5 \times 10^{-7}$ esu [24]. The experimental studies where the value and sign of both the real and imaginary components of $\chi^{(3)}$ could be determined (by the z-scan or other techniques providing the modulus and the phase of the susceptibility) have already demonstrated the dominance of $\mathrm{Im}\chi^{(3)}$ over $\mathrm{Re}\chi^{(3)}$ close to the SPR, with a negative sign for the imaginary part [4,5,9,15,16,24] (except in Ref. [10] where the composite medium absorption coefficient β is found to be positive for Au:SiO_2 and Cu:SiO_2 cermets synthesized by ion-implantation). Among these studies, those for which the metal concentration of the cermets or colloidal solutions is low have shown, by using equation (7) which is valid in this case, that at or close to the SPR the imaginary part of the particle third-order susceptibility $\chi^{(3)}_{\mathrm{m}}$ is positive, whatever possible size effects [4, 5,9,16]. As stated before, such a determination of $\chi^{(3)}_{\mathrm{m}}$ is forbidden in our case, due to the lack of knowledge about the actual local field enhancement factor linked with the high p values.

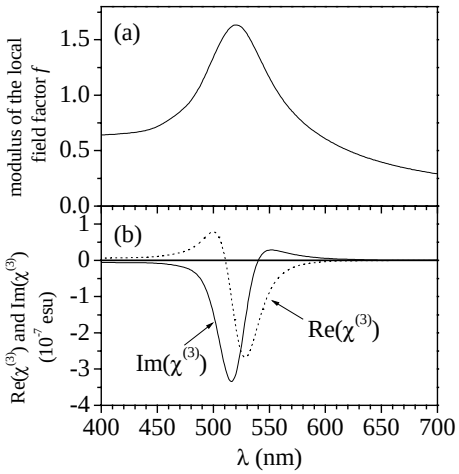

Fig. 4. Spectral variations of (a) the modulus of the local field factor f as given by equation (8) and (b) the real and imaginary parts of $\chi^{(3)}$, calculated with the dilute media theory (Eq. (7)) for an Au:SiO_2 cermet with $p = 10\%$.

Results similar to those reported in Figure 3 were already reported at $\lambda = 532$ nm by Liao *et al.* on Au:SiO_2 cermets prepared by cosputtering and annealed at 850 °C over a very wide range of metal concentrations [13]. However, as their experiment is based on the DFWM technique, it only provides the variation of the modulus of the third-order susceptibility, $|\chi^{(3)}|$, whereas in the present paper we prove the material nonlinearity to be essentially imaginary and negative for all concentrations and at this wavelength. Moreover, in their experiment, the mean particle size variation with metal concentration is so large

(mean diameter from 3 to 80 nm) that is renders the interpretation of the nonlinear response dependence on p less obvious. Nevertheless, they clearly show that $|\chi^{(3)}|$ reaches a maximum near the percolation threshold while increasing p. We expect our highest-concentrated sample (sample D, $p = 35\%$) to be very close from this optical percolation threshold (see also the linear response behavior, Fig. 2, and the discussion in Sect. 3).

When comparing our results for $|\chi^{(3)}|$ on annealed samples with those obtained by Liao *et al.* at equivalent metal concentrations, we find our values to be significantly higher [13]. This has been explained by the possible role played by thermal effects in the nonlinear optical response of the metal nanoparticles depending on the temporal regime of the excitation light [18] (the pulse duration is 70 ps in Ref. [13], against 7 ns in the present case). Further considerations regarding such phenomena are out of the scope of this paper but will form the subject of a subsequent publication. Let us just notice that any thermal effect should not only be governed by the laser pulse duration, but also by its peak intensity and repetition rate (possible processes of thermal energy accumulation in the medium) [8,12,22].

Another characteristic exhibited by the theoretical prediction shown in Figure 4b is that the amplitude of both the real and imaginary components of $\chi^{(3)}$ should undergo strong spectral variations around the SPR, as well as sign reversal. In particular, these components are expected to be very weak quite far from the SPR maximum wavelength. In the aim to validate this assumption, z-scan measurements have also been performed on each sample (except sample D) at $\lambda = 600$ nm by using a dye oscillator pumped by a frequency-doubled Nd-YAG laser. Indeed, this wavelength is located in the red wing limit of the SPR band, as it can be seen in Figure 2b (where the excitation wavelength is indicated by an arrow), and the local field enhancement is, therefore, very weak. The measurements reveal too weak $\mathrm{Im}\chi^{(3)}$ and $\mathrm{Re}\chi^{(3)}$ values to be significantly extracted from noise with our apparatus sensitivity. This result confirms the link between the large value of $|\chi^{(3)}|$ and the local field enhancement at the SPR, as well as the strong amplitude variations of $\chi^{(3)}$ in the SPR spectral domain. DFWM experiment results reported in the literature have already pointed out such spectral dependence of $|\chi^{(3)}|$ (the profile of the third-order susceptibility modulus roughly following the linear absorbance spectrum profile) [11,14,18]; however, no measurement has yet been published, to our knowledge, regarding the spectral variation of the real and imaginary parts of $\chi^{(3)}$ separately. Experimental investigation is in progress in our group to explore in more details these variations and to detect sign reversal, if any.

5 Conclusion

Au:SiO_2 cermet films with high metal volume fraction under the percolation threshold have been prepared by RF sputtering. The sample structural and optical properties have been particularly investigated in order to interpret the nonlinear response. Z-scan measurements have revealed a large negative $\mathrm{Im}\chi^{(3)}$ value in the vicinity of the SPR, increasing with metal concentration with a rate highly larger than the simple linear law predicted by a mean field theory, the latter being suited only for weakly concentrated materials. These results have highlighted the need to take exactly into account the local spatial variations of the electromagnetic field when mutual interactions between particles cannot be neglected.

Moreover, we have observed a strong correlation between the film morphologic properties and the optical ones, especially for the nonlinear response. Indeed, after sample annealing – which cancels lattice defects in the particles and increases both their size and the total amount of "optically active" metal by favoring the diffusion and coalescence of isolated atoms and very small particles –, the absolute value of $\mathrm{Im}\chi^{(3)}$ rises remarkably.

Finally, we have experimentally shown that the amplitude of the nonlinear response strongly depends on the excitation wavelength in the SPR domain, as qualitatively expected from the predictions of the usual mean field theory (Fig. 4). These amplitude variations – as well as sign reversal – for both the real and imaginary parts of $\chi^{(3)}$ yield to consider nanocermets as valuable potential candidates for optically-driven switching in optical telecommunications. Indeed, provided the SPR being shifted in the near-infrared domain by, for instance, synthesizing elongated particles [43], large $|\mathrm{Re}\chi^{(3)}|$ values can be generated by slightly detuning the excitation wavelength from the SPR maximum, while taking advantage of a large negative nonlinear absorption increasing the medium transparency.

The authors thank C. Sella for his invaluable assistance in the film synthesis. They are grateful to A. Brunet-Bruneau for RBS measurements and fruitful discussions. We would like also to thank C. Ricolleau (LMCP, Paris) for his collaboration in the TEM studies and A. Naudon (LMP, Poitiers) for GISAXS measurements performed at LURE facility (Orsay).

References

1. See U. Kreibig, M. Vollmer, *Optical properties of metal clusters* (Springer, Berlin, 1995) and references therein.
2. D. Ricard, P. Roussignol, C. Flytzanis, Opt. Lett. **10**, 511 (1985).
3. F. Hache, D. Ricard, C. Flytzanis, J. Opt. Soc. Am. B **3**, 1647 (1986).
4. F. Hache, D. Ricard, C. Flytzanis, U. Kreibig, Appl. Phys. A **47**, 347 (1988).
5. M.J. Bloemer, J.W. Haus, P.R. Ashley, J. Opt. Soc. Am. B **7**, 790 (1990).
6. K. Fukumi, A. Chayahara, K. Kadono, T. Sakaguchi, Y. Horino, M. Miya, J. Hayakawa, M. Satou, Jpn J. Appl. Phys. **30**, 742 (1991).
7. K. Fukumi, A. Chayahara, K. Kadono, T. Sakaguchi, Y. Horino, M. Miya, K. Fujii, J. Hayakawa, M. Satou, J. Appl. Phys. **75**, 3075 (1994).
8. R.H. Magruder III, R.F. Haglund Jr, L. Yang, J.E. Wittig, R.A. Zuhr, J. Appl. Phys. **76**, 708 (1994).
9. K. Puech, F. Henari, W. Blau, D. Duff, G. Schmid, Europhys. Lett. **32**, 119 (1995).

10. L. Yang, D.H. Osborne, R.F. Haglung Jr, R.H. Magruder, C.W. White, A. Zuhr, H. Hosono, Appl. Phys. A **62**, 403 (1996).
11. I. Tanahashi, Y. Manabe, T. Tohda, S. Sasaki, A. Nakamura, J. Appl. Phys. **79**, 1244 (1996).
12. S.C. Mehendale, S.R. Mishra, K.S. Bindra, M. Laghate, T.S. Dhami, K.C. Rustagi, Opt. Commun. **133**, 273 (1997).
13. H.B. Liao, R.F. Xiao, J.S. Fu, P. Yu, G.K.L. Wong, Ping Sheng, Appl. Phys. Lett. **70**, 1 (1997).
14. Y. Hosoya, T. Suga, T. Yanagawa, Y. Kurokawa, J. Appl. Phys. **81**, 1475 (1997).
15. J.M. Ballesteros, R. Serna, J. Solis, C.N. Afonso, A.K. Petford-Long, D.H. Osborne, R.F. Haglund Jr, Appl. Phys. Lett. **71**, 2445 (1997).
16. D.D. Smith, G. Fisher, R.W. Boyd, D.A. Gregory, J. Opt. Soc. Am. B **14**, 1625 (1997).
17. H.B. Liao, R.F. Xiao, J.S. Fu, G.K.L. Wong, Appl. Phys. B **65**, 673 (1997).
18. H.B. Liao, R.F. Xiao, J.S. Fu, H. Wang, K.S. Wong, G.K.L. Wong, Opt. Lett. **23**, 388 (1998).
19. H. Inouye, K. Tanaka, I. Tanahashi, K. Hirao, Jpn J. Appl. Phys. **37**, L1520 (1998).
20. M. Falconieri, G. Salvetti, E. Cattaruzza, F. Gonella, G. Mattei, P. Mazzoldi, M. Piovesan, G. Battaglin, R. Polloni, Appl. Phys. Lett. **73**, 288 (1998).
21. L. Guo, Z.H. Wu, K. Ibrahim, T. Liu, Y. Tao, X. Ju, Eur. Phys. J. D **9**, 591 (1999).
22. J.M. Ballesteros, J. Solis, R. Serna, C.N. Afonso, Appl. Phys. Lett. **74**, 2791 (1999).
23. L. Gao, Z.Y. Li, J. Appl. Phys. **87**, 1620 (2000).
24. S. Debrus, J. Lafait, M. May, N. Pinçon, D. Prot, C. Sella, J. Venturini, J. Appl. Phys. **88**, 4469 (2000).
25. K. Puech, W.J. Blau, J. Nanopart. Res. **3**, 13 (2001).
26. M. Sheik-Bahae, A.A. Said, T. Wei, D.J. Hagan, E.W. van Stryland, IEEE J. Quant. Electron. **26**, 760 (1990).
27. C. Sella, M. Maaza, B. Pardo, F. Dunsteter, J.C. Martin, M.C. Sainte-Catherine, Physica A **241**, 192 (1997).
28. A. Dakka, J. Lafait, C. Sella, S. Berthier, M. Abd-Lefdil, J.-C. Martin, M. Maaza, Appl. Opt. **39**, 2745 (2000).
29. A. Naudon, D. Babonneau, Z. Metall. **88**, 596 (1997).
30. A. Gibaud, S. Hazra, C. Sella, P. Laffez, A. Désert, A. Naudon, G. van Tendeloo, Phys. Rev. B **63**, 193407 (2001).
31. L. Yang, G.H. Li, L.D. Zhang, Appl. Phys. Lett. **76**, 1537, (2000).
32. E. Duval, H. Portales, L. Saviot, M. Fuji, K. Sumitomo, S. Hayashi, Phys. Rev. B **63**, 075405 (2001).
33. B. Palpant, B. Prével, J. Lermé, E. Cottancin, M. Pellarin, M. Treilleux, A. Perez, J.-L. Vialle, M. Broyer, Phys. Rev. B **57**, 1963 (1998).
34. J. Lermé, B. Palpant, B. Prével, M. Pellarin, M. Treilleux, J.-L. Vialle, A. Perez, M. Broyer, Phys. Rev. Lett. **80**, 5105 (1998).
35. J.C. Maxwell-Garnett, Philos. Trans. R. Soc. Lond. **203**, 385 (1904); **205**, 237 (1906).
36. D.A.G. Bruggeman, Ann. Phys. (Lpz.) **24**, 636 (1935).
37. S. Berthier, *Optique des Milieux Composites* (Polytechnica, Paris, 1993).
38. C.G. Granqvist, O. Hunderi, Phys. Rev. B **16**, 3513 (1977).
39. U. Kreibig, Z. Phys. B **31**, 39 (1978).
40. D.D. Smith, Y. Yoon, R.W. Boyd, J.K. Campbell, L.A. Baker, R.M. Crooks, M. George, J. Appl. Phys. **86**, 6200 (1999).
41. V.M. Shalaev, A.K. Sarychev, Phys. Rev. B **57**, 13265 (1998).
42. P. Gadenne, X. Quelin, S. Ducourtieux, S. Gresillon, L. Aigouy, J.-C. Rivoal, V. Shalaev, A. Sarychev, Physica B **279**, 52 (2000).
43. S. Link, M.B. Mohamed, M.A. El-Sayed, J. Phys. Chem. B **103**, 3073 (1999).